An Alternative Explicit and Unconditionally Stable Time-Domain Finite-Element Method for Electromagnetic Analysis

Woochan Lee, *Member, IEEE*, and Dan Jiao, *Fellow, IEEE*

***Abstract*—A new method for making an explicit time-domain finite-element method unconditionally stable is developed for general electromagnetic analysis, where the dielectrics and conductors can be inhomogeneous, lossless, or lossy. In this method, for a given time step, we find the unstable modes that are the root cause of instability, and deduct them directly from the system matrix resulting from a time-domain finite-element based analysis. The resultant explicit time-domain simulation is absolutely stable for the given time step no matter how large it is, and irrespective of the space step. The accuracy of the method is also guaranteed when the time step is chosen based on accuracy. In addition to a formulation for lossless problems, formulations for general lossy problems are also presented in detail. Numerical experiments have demonstrated the accuracy, efficiency, and unconditional stability of the proposed new explicit method.**

***Index Terms*—Electromagnetic analysis, explicit methods, time-domain finite-element method (TDFEM), transient analysis, unconditionally stable schemes.**

I. Introduction

TIME-DOMAIN methods are of critical importance for analyzing transient and nonlinear physical phenomena. Among existing time-domain methods, explicit methods can avoid solving a matrix equation. However, their time step is traditionally restricted by the space step for ensuring the stability of a time-domain simulation, such as the well-known Courant-Friedrichs-Lewy (CFL) condition required by an explicit finite-difference time-domain (FDTD) method, and a similar condition in a time-domain finite-element method (TDFEM) [1]. Because of the dependence of time step on space step, when the structure being simulated involves fine features relative to the working wavelength, a tremendous number of time steps are required to finish one simulation, which is computationally expensive. Indeed, some of the fine features, even though they physically exist, can be safely ignored without affecting much the overall solution accuracy. However, there are also fine features that must be captured to obtain a correct solution of the original problem. The latter is the problem studied in this work, and also in other works that aim to break the time step limit such as [2]–[8].

An unconditionally stable time domain method eliminates the dependence of time step on space step. It also permits the use of an arbitrarily large time step without making a time-domain simulation unstable. Existing unconditionally stable methods are mainly implicit methods such as [2]–[8]. Unlike explicit methods that can avoid solving a matrix equation, an implicit method requires a matrix solution, and hence becoming computationally expensive when the matrix size is large. Furthermore, the accuracy of an implicit method degrades with the increase of time step. Late time instability has also been observed in implicit unconditionally stable methods [11]. In addition to implicit methods, spatial filtering techniques have also been developed to extend the CFL limit of the FDTD [9], [10].

Recently in [11], an explicit and unconditionally stable TDFEM is created. The essential idea of this method is very different from that of an implicit method for achieving unconditional stability. In an implicit method, the source of instability is not removed. Instead, a different time integration technique is employed to suppress the instability. Among the implicit methods, not all of them are unconditionally stable. If the time integration technique does not bound the error amplification factor to be one, the resulting implicit method can still be unstable. In the newly developed explicit and unconditionally stable TDFEM method [11], the time integration scheme remains the same as that of an explicit time marching scheme. However, the source of instability is found, and subsequently eradicated from the numerical system of an explicit time marching. As a result, an explicit time marching can also be made unconditionally stable.

By comparing the new explicit unconditionally stable method with the implicit method in both dispersion error and total solution error [12], it has also been found that the degradation of an implicit method in accuracy and late-time stability can be attributed to the unremoved source of instability. This source is, in fact, the eigenmodes present in the field solution, which however cannot be accurately simulated by the given time step. Although these eigenmodes are suppressed to be stable by an implicit time integration technique, they can still negatively affect the overall accuracy and stability of a time-domain solution. On the contrary, by removing these unstable modes altogether like what is fulfilled in [11]–[13], the remaining eigenmodes comprising the field solution can all be accurately simulated by the given time step, and hence ensuring not only stability but also accuracy.

Manuscript received July 18, 2017; revised October 19, 2017 and January 10, 2018; accepted February 22, 2018. Date of publication March 9, 2018; date of current version April 24, 2018. This work was supported in part by the NSF under Grant 1065318, in part by the Intel Corporation under a grant, and in part by DARPA under Grant N00014-10-1-0482B. *(Corresponding author: Dan Jiao.)*

W. Lee is with the Department of Electrical Engineering, Incheon National University, Incheon 406-772, South Korea (e-mail: wlee@inu.ac.kr).

D. Jiao is with the School of Electrical and Computer Engineering, Purdue University, West Lafayette, IN 47907 USA (e-mail: djiao@purdue.edu).

Digital Object Identifier 10.1109/JMMCT.2018.2814480

It is also worth mentioning that for a general inhomogeneous problem, the eigenmodes found in [11]–[13] are not spatial Fourier modes used in Von Neumann analysis and filtering techniques [9], [10], and their eigenvalues are not spatial frequencies. Instead, each of the eigenmodes is a source-free solution of the given problem satisfying all the boundary conditions at the material interfaces. Therefore, not only the unstable eigenmodes, whose eigenvalues are the highest, but also the stable eigenmodes capture the fine features present in the structure, including the lowest eigenmodes whose eigenvalues are zero. If one takes a single eigenmode and performs a spatial Fourier transform on it, he would get a range of spatial frequencies from low to very high. For example, the zero-eigenvalue mode, which is a static field distribution, also captures the rapid space variation of the field surrounding fine features. The unstable eigenmodes in [11]–[13] are removed based on their negligible weights in the field solution, which are analytically known from their eigenvalues λ_i and the working frequency ω. For example, in a lossless problem, this weight is proportional to $1/(\lambda_i - \omega^2)$. The unstable modes have the largest eigenvalues beyond those that can be accurately simulated by a given time step. Since their weights are negligible for the input spectrum, removing them does not affect the accuracy. It should be emphasized that removing unstable modes in the methods of [11]–[13] is not the same as removing the high spatial Fourier modes since the two sets of modes are different. Hence, it is not the same as ignoring the fine features or fields with fast space variations. In the proposed method and [11]–[13], the stable eigenmodes that are kept in the simulation have also captured the fine features, thus, the fast space variations of the field. It is true that without fine features, the unstable modes would not exist. However, with the fine features, not only the unstable modes but also the stable modes capture the fine features. In other words, the stable modes are obtained subject to the presence of the fine features. With or without the fine features, the stable eigenmodes are different, and their eigenvalues do not correspond to the frequency of the space variation. No matter how fine the spatial feature can be, the eigenvalue of an eigenmode in this fine structure can be as small as zero, but still capturing the fine feature like the zero-eigenvalue mode (dc mode).

In [11], for any given time step Δt, the root cause of the instability for lossless problems is analytically found to be the eigenmodes of the system matrix whose eigenvalues are higher than $4/\Delta t^2$. The method in [11] begins with a preprocessing step that finds the space of stable eigenmodes followed by an explicit time marching stable for the given time step no matter how large it is. To preserve the advantage of an explicit time-domain method in avoiding solving a matrix equation, the preprocessing step is performed by using the conventional explicit marching. Although the time window to be simulated in the preprocessing can be much shorter than the total window to be simulated, the performance of the preprocessing step may become limited in certain applications. The same is true to the FDTD methods developed in [12], [13].

In this paper, we propose a new method for achieving unconditional stability in an explicit TDFEM. In this new method, for a given time step, we find the unstable modes, and directly deduct them from the system matrix resulting from the TDFEM analysis. In other words, we adapt the underlying numerical system based on the given time step to eradicate the source of instability. We then perform an explicit time marching on the updated numerical system that is free of unstable modes. The resultant explicit simulation is absolutely stable for the given time step irrespective of its size as well as the space step. Meanwhile, the conventional explicit time marching based preprocessing step required by [11] is eliminated in this new method. Furthermore, we present algorithms for analyzing general lossy problems where both dielectrics and conductors can be lossy and inhomogeneous. Such a general lossy problem has not been analyzed in [11], [13], while [12] requires finding stable modes from a preprocessing step. Since a general lossy problem is governed by a quadratic eigenvalue problem with complex-valued eigenvalues and eigenmodes, it is not straightforward to extend a method for analyzing lossless problems to analyze general lossy problems. New algorithms need to be developed to make an explicit TDFEM unconditionally stable for analyzing general lossy problems. This makes the other focus of this paper. Compared to our conference paper [18], in this work, we develop complete algorithms for both lossless and lossy problems. For lossy problems, we also provide a theoretical analysis on how the algorithm works, propose another explicit marching scheme, and a scaling algorithm that improves accuracy. In addition, more numerical examples are simulated.

The remainder of this paper is organized as follows. In Section II, we review the root cause of instability of an explicit time-domain method. In Section III, we present the proposed method for analyzing the lossless problems; in Section IV, we describe the proposed method for analyzing general lossy problems. Section V provides abundant examples to validate the accuracy, efficiency, and unconditional stability of the proposed methods. Section VI concludes this paper.

II. Review on the Root-Cause of Instability

Consider Maxwell's equations governing a general problem having space-dependent conductivity σ, permittivity ε, and permeability μ in a source-free region. A time-domain FEM solution of such a problem results in the following linear system of equations

$$\mathbf{T}\ddot{u}(t) + \mathbf{R}\dot{u}(t) + \mathbf{S}u(t) = \dot{I}(t) \tag{1}$$

in which $\mathbf{T}$ is a mass matrix, $\mathbf{R}$ is related to conductivity, $\mathbf{S}$ is a stiffness matrix, u is a vector containing all field unknowns in the computational domain, and I denotes a vector of the current sources. The single dot above a letter in (1) represents a first-order time derivative, while the double dots signify a second-order time derivative. The $\mathbf{T}$, $\mathbf{R}$, and $\mathbf{S}$ are assembled from their elemental contributions as the following:

$$\mathbf{T}^e = \mu_0 \varepsilon \langle \mathbf{N}_i, \mathbf{N}_j \rangle \tag{2}$$

$$\mathbf{R}^e = \mu_0 \sigma \langle \mathbf{N}_i, \mathbf{N}_j \rangle \tag{3}$$

$$\mathbf{S}^e = {\mu_{\mathrm{r}}}^{-1} \langle \nabla \times \mathbf{N}_i, \nabla \times \mathbf{N}_j \rangle \tag{4}$$

where μ_0 is the free-space permeability, μ_{r} is the relative permeability, $\boldsymbol{N}$ is the vector basis function employed to expand electric field $\mathbf{E}$ in each element, and $\langle \cdot, \cdot \rangle$ denotes an inner product. A central-difference-based time discretization of (1), which is an explicit scheme, results in the following system of

equations:

$$\left\{\frac{1}{(\Delta t)^2}\mathbf{T}+\frac{1}{2\Delta t}\mathbf{R}\right\}u^{n+1} = \left\{\frac{2}{(\Delta t)^2}\mathbf{T}-\mathbf{S}\right\}u^{n}-\left\{\frac{1}{(\Delta t)^2}\mathbf{T}-\frac{1}{2\Delta t}\mathbf{R}\right\}u^{n-1}-\dot{I}^{n}. \tag{5}$$

The solution of (1) is governed by the following quadratic eigenvalue problem:

$$(\lambda^2\mathbf{T}+\lambda\mathbf{R}+\mathbf{S})V=0 \tag{6}$$

in which λ denotes eigenvalues, and V is the eigenvector. The eigenvectors of (6) form a complete space to represent the field solution's space dependence. This is because there are N linearly independent eigenvectors of (6) [14]. The solution of (1) at any time is hence nothing but a linear superposition of the eigenvectors of (6) as the following:

$$u(t)=\mathbf{V}y(t)=\sum_i V_i y_i(t) \tag{7}$$

with the weight of each eigenvector, y_i, being time dependent.

For lossless cases where $\mathbf{R}$ is absent, (6) can be simplified as a generalized eigenvalue problem

$$\mathbf{S}V=\xi\mathbf{T}V \tag{8}$$

where eigenvalues ξ are real and nonnegative, since $\mathbf{T}$ is Hermitian positive definite, and $\mathbf{S}$ is Hermitian positive semidefinite. In [11], it is shown that the root cause of the instability of (5), for any given time step Δt, is the eigenmodes of (8) that have the following eigenvalues:

$$\sqrt{\xi_i}>\frac{2}{\Delta t}, i\in(1,N). \tag{9}$$

These eigenmodes are termed unstable modes for the given time stepΔt.

For general lossy cases where $\mathbf{R}$ is present, the eigenvalues of (6) come into pairs. They are either no greater than zero, i.e., negative real or zero, or complex conjugates of each other [14]. This is because $\mathbf{T}$ is Hermitian positive definite, $\mathbf{R}$ and $\mathbf{S}$ are Hermitian and positive semidefinite. Consider a source-free problem for stability analysis. As theoretically derived in [12], if the two eigenvalues in an eigenvalue pair are both negative but different, the time-dependence of their corresponding eigenmodes is an exponential decay with time; if the two eigenvalues are both negative but identical, the time-dependence of their corresponding eigenmodes represents a critically damped case; if the two eigenvalues are complex conjugates of each other, they correspond to an under-damped time dependence. In [12], for all of these three cases, a detailed root cause analysis of the instability is conducted, and it is found that the eigenmodes of (6) that have the following eigenvalues:

$$\sqrt{|\lambda_{i1}\lambda_{i2}|}>\frac{2}{\Delta t}, i\in(1,N) \tag{10}$$

cannot be stably simulated by the given time step in a central-difference-based explicit time marching, and hence they are the root cause of instability. In (10), λ_{i1} and λ_{i2} represent a pair of eigenvalues of (6). Obviously, (10) is more general for use since (9) is a special case of (10).

There are a few important findings that can be drawn from (10). First, when an explicit time-domain method becomes unstable for a given time step, not all the eigenmodes comprising the field solution are unstable; there always exists a set of eigenmodes that can be stably simulated. This is because the smallest eigenvalues of (6) and (8) are zero. The zero eigenvalues as well as nonzero ones not satisfying (10) can be stably simulated by the given time step no matter how large the time step is. The second finding is on why the unstable modes exist. They exist because of fine space discretizations relative to the working wavelength. The finer the space discretization, the larger the largest eigenvalue of (6). The fine discretizations cannot be avoided in a structure having fine features relative to working wavelengths. Third, the unstable modes are also those eigenmodes that cannot be accurately simulated by the given time step. To see this point clearly, in lossless cases, the $y_i(t)$ in (7) of an eigenmode, whose eigenvalue is ξ_i, is analytically known as

$$y_i(t)=A\cos(\sqrt{\xi_i}t)+B\sin(\sqrt{\xi_i}t) \tag{11}$$

in a source-free problem, where A and B are arbitrary coefficients. In lossy cases, as shown in [12], the $y_i(t)$ has the following three forms:

$$y_i(t)=\begin{cases} Ae^{\lambda_{i1}t}+Be^{\lambda_{i2}t} \\ (A+Bt)e^{\lambda_i t} \\ e^{\mathrm{Re}[\lambda_i]t}\left[A\cos(\mathrm{Im}[\lambda_i]t)+B\sin(\mathrm{Im}[\lambda_i]t)\right]. \end{cases} \tag{12}$$

When (10) holds true, the time variation of the specific eigenmode is too high to be accurately sampled by the given time step, and hence causing instability. Last and also the most important, when the time step is chosen based on accuracy, the unstable modes are not required by accuracy. Hence, they can be removed without sacrificing accuracy. A detailed analysis can be found in [11]–[13]. To give a simple explanation, when Δt is chosen based on accuracy, it generally satisfies $\Delta t\le 1/(10f_{\max})$, where $f_{\max}$ is the maximum frequency corresponding to the smallest wavelength present in the problem being simulated. The unstable modes have eigenvalues satisfying (10), and hence $|\lambda_i|>20f_{\max}>2\pi f_{\max}$. Based on the Fourier transform of either (11) or (12), it is evident that such a λ_i is beyond the maximum frequency required by accuracy. Both (11) and (12) are source-free solutions. When sources are present, take a lossless problem as an example, the field solution for a source vector b can be written as $u(\omega)=\sum_i \frac{1}{\xi_i-\omega^2}V_iV_i^T b$in frequency domain [11]. Thus, for a band limited input, there is a maximum eigenvalue ξ_i we need to capture for a prescribed accuracy, which determines the smallest wavelength. The unstable modes have eigenvalues larger than that, and hence can be removed without sacrificing the prescribed accuracy.

III. Proposed Method for Lossless Problems

Consider a general lossless problem, in a traditional explicit time-domain method, the time step is chosen in the following way:

$$\Delta t<\frac{2}{|\lambda|_{\max}} \tag{13}$$

that is based on the largest eigenvalue of (6), $|\lambda|_{\max}$, so that all eigenmodes comprising the field solution can be stably simulated by the given time step. Since $|\lambda|_{\max}$ is inversely propor-

tional to the smallest space step, the time step of a traditional explicit method is restricted by the smallest space step. In the proposed explicit method, instead of choosing a time step to make the explicit simulation stable, we fix the time step to be the desired value, but choose the eigenmodes that can be stably simulated by the given time step as the following:

$$|\lambda_i| < \frac{2}{\Delta t} \tag{14}$$

while discarding the unstable modes. As a result, the time step no longer depends on space step, and an explicit time-domain method can also be made unconditionally stable. Meanwhile, the accuracy is ensured when the time step is chosen based on accuracy.

In this section, we present an alternative explicit and unconditionally stable TDFEM, which is different from [11] as well as [12], for analyzing general lossless problems.

A. Method

Let $\mathbf{V}_h$ denote the matrix whose column vectors are the eigenvectors of (8) having eigenvalues satisfying (9). $\mathbf{V}_h$ thus contains all the unstable modes for the given time step.

We update the original system of equations (1) to a new system of equations as the following:

$$\mathbf{T}\ddot{u}(t) + \mathbf{S}\left(\mathbf{I} - \mathbf{V}_h\mathbf{V}_h^T\mathbf{T}\right)u(t) = \dot{I}(t) \tag{15}$$

where $\mathbf{S}$ is changed to $\mathbf{S}(\mathbf{I} - \mathbf{V}_h\mathbf{V}_h^T\mathbf{T})$.

We then perform a central-difference-based explicit time marching of (15) as the following:

$$\tilde{u}^{n+1} = \left\{2 - \Delta t^2\mathbf{T}^{-1}\mathbf{S}\left[\mathbf{I} - \mathbf{V}_h\mathbf{V}_h^T\mathbf{T}\right]\right\}u^n - u^{n-1} + \Delta t^2\mathbf{T}^{-1}\dot{I}^n \tag{16}$$

in which superscripts $n-1$, n, $n+1$ denote time instants.

Obviously, the only extra computation involved in (16), as compared to the traditional TDFEM, is the evaluation of $\mathbf{V}_h\mathbf{V}_h^T\mathbf{T}u^n$ term. This term can be efficiently evaluated by three matrix-vector multiplications performed in sequence from right to left: First, sparse matrix-vector multiplication $\mathbf{T}u^n$; then a multiplication of the resultant vector by $\mathbf{V}_h^T$, followed by another multiplication with $\mathbf{V}_h$. The total computational cost is $O(kN)$, where k is the number of the unstable modes.

At each time step, after obtaining the field solution $\tilde{u}^{n+1}$ via (16), we need to add one important step as shown below to make the solution correct

$$u^{n+1} = \tilde{u}^{n+1} - \mathbf{V}_h\mathbf{V}_h^T\mathbf{T}\tilde{u}^{n+1}. \tag{17}$$

B. How it Works?

Now, we shall prove the correctness of the aforementioned method. The method essentially changes the original numerical system consisting of both the unstable and stable modes to a system of stable modes only. To prove, the solution of (16) is now governed by the eigen-solution of a new system matrix $\mathbf{T}^{-1}\mathbf{S}(\mathbf{I} - \mathbf{V}_h\mathbf{V}_h^T\mathbf{T})$instead of the original $\mathbf{T}^{-1}\mathbf{S}$. For convenience, let us denote $\mathbf{T}^{-1}\mathbf{S}(\mathbf{I} - \mathbf{V}_h\mathbf{V}_h^T\mathbf{T})$ by

$$\mathbf{M}_{\text{new}} = \mathbf{T}^{-1}\mathbf{S}\left(\mathbf{I} - \mathbf{V}_h\mathbf{V}_h^T\mathbf{T}\right) \tag{18}$$

in contrast to the original system matrix denoted by

$$\mathbf{M} = \mathbf{T}^{-1}\mathbf{S}. \tag{19}$$

Let $\mathbf{V}$ be the matrix whose column vectors are the eigenvectors of $\mathbf{M}$, which is the union of the unstable eigenmodes $\mathbf{V}_h$ that satisfy (9), and the stable ones $\mathbf{V}_s$ that do not satisfy (9). Thus,

$$\mathbf{V} = [\mathbf{V}_s\ \mathbf{V}_h]. \tag{20}$$

Since (8) is a symmetric definite eigenvalue problem as $\mathbf{T}$ is symmetric positive definite, and $\mathbf{S}$ is symmetric positive semidefinite, the following property holds true:

$$\mathbf{V}^T\mathbf{T}\mathbf{V} = \mathbf{I} \tag{21}$$

in which $\mathbf{I}$ is an identity matrix. We hence can deduce

$$\mathbf{V}^{-1} = \mathbf{V}^T\mathbf{T} = \begin{bmatrix}\mathbf{V}_s^T\mathbf{T}\\ \mathbf{V}_h^T\mathbf{T}\end{bmatrix}. \tag{22}$$

From (8), the original system matrix $\mathbf{M} = \mathbf{T}^{-1}\mathbf{S}$ can be written as

$$\mathbf{M} = \mathbf{V}\Lambda\mathbf{V}^{-1} \tag{23}$$

where Λ is the diagonal matrix of all the eigenvalues. Substituting (20) and (22) into (23), we obtain

$$\mathbf{M} = \mathbf{V}_s\Lambda_s\mathbf{V}_s^T\mathbf{T} + \mathbf{V}_h\Lambda_h\mathbf{V}_h^T\mathbf{T}. \tag{24}$$

Clearly, $\mathbf{M}$ has two components: one component in $\mathbf{V}_s$ space, and the other in$\mathbf{V}_h$ space. Here, $\Lambda_s$denotes the diagonal matrix containing the eigenvalues of the stable modes in $\mathbf{V}_s$, and Λ_h is the diagonal matrix of the eigenvalues of the unstable modes.

From (18), the new system matrix is

$$\mathbf{M}_{\text{new}} = \mathbf{M} - \mathbf{M}\mathbf{V}_h\mathbf{V}_h^T\mathbf{T}. \tag{25}$$

Substituting (24) into it, and utilizing the property of (20) which yields $\mathbf{V}_s^T\mathbf{T}\mathbf{V}_h = 0$ and $\mathbf{V}_h^T\mathbf{T}\mathbf{V}_h = \mathbf{I}$, we obtain

$$\mathbf{M}_{\text{new}} = \mathbf{V}_s\mathbf{\Lambda}_s\mathbf{V}_s^T\mathbf{T} \tag{26}$$

which is nothing but the first term of $\mathbf{M}$ in (24), and hence the component of $\mathbf{M}$ in the stable space. Multiplying both sides of (26) from right by $\mathbf{V}_s$, using (21), it is evident that

$$\mathbf{M}_{\text{new}}\mathbf{V}_s = \mathbf{V}_s\mathbf{\Lambda}_s. \tag{27}$$

Therefore, $(\mathbf{\Lambda}_s, \mathbf{V}_s)$ is the eigen-pair of the new system matrix $\mathbf{M}_{\text{new}}$. Hence, the explicit marching based on $\mathbf{M}_{\text{new}}$, as shown in (16), is absolutely stable for the given time step no matter how large it is. As a result, we prove the unconditional stability of (16) irrespective of space step.

Although (16) is absolutely stable for the given time step, we found the solution obtained from (16) is not correct. To make the solution correct, we need to add one more important step shown in (17). This is because the new system matrix $\mathbf{M}_{\text{new}}$ has not only stable eigenmodes $\mathbf{V}_s$ of the original system matrix $\mathbf{M}$, but also an additional nullspace. This can be readily seen from (26). The rank of (26) and thereby $\mathbf{M}_{\text{new}}$ is the number of stable eigenmodes, denoted by k_s, while the matrix size of (26) is N. $\mathbf{M}_{\text{new}}$ is therefore a low-rank matrix with (N-k_s) additional zero eigenvalues, in addition to the k_s eigenvalues of the stable eigenmodes. The solution of (16) is thus the superposition of not only the stable eigenmodes $\mathbf{V}_s$, but also the eigenvectors in the additional nullspace. We can write the solution of (16) as

$$u = \mathbf{V}_s y_s + \mathbf{V}_{a0} y_{a0} \tag{28}$$

where $\mathbf{V}_{a0}$ denotes the additional nullspace of $\mathbf{M}_{\text{new}}$, y_s, and y_{a0} are the coefficient vectors for $\mathbf{V}_s$ modes, and $\mathbf{V}_{a0}$ modes, respectively. This additional nullspace $\mathbf{V}_{a0}$is different from the

nullspace of the original system matrix $\mathbf{M}$. Although it can be simulated stably in (16) since its eigenvalues are zero, it makes the solution of (16) incorrect, as numerically they are not exact zeros.

The treatment of (17) effectively removes the second term in the right hand side of (28), i.e., the contribution from $\mathbf{V}_{a0}$ nullspace. This is because when we multiply (28) by $\mathbf{V}_h\mathbf{V}_h^T\mathbf{T}$, since $\mathbf{V}_h^T\mathbf{T}\mathbf{V}_s = 0$, the first term in the right hand side of (28) vanishes, leaving the second term only. $\mathbf{V}_h\mathbf{V}_h^T\mathbf{T}u$ thus becomes nothing but

$$\mathbf{V}_h\mathbf{V}_h^T\mathbf{T}u = \mathbf{V}_h\mathbf{V}_h^T\mathbf{T}\mathbf{V}_{a0}y_{a0} = \mathbf{V}_h y_h \tag{29}$$

that is the $\mathbf{V}_h$-component of u. As a consequence, the treatment of (17) deducts the $\mathbf{V}_h$-component from u, leaving only the $\mathbf{V}_s$-component, and hence making the solution of (16) correct.

Interestingly, we also found that if we perform a full eigenvalue analysis of $\mathbf{M}$ to determine $\mathbf{V}_h$, and then deduct it from $\mathbf{M}$, (16) by itself can yield a correct solution. However, for the sake of computational efficiency, if we find $\mathbf{V}_h$ modes only instead of finding all eigenvectors of $\mathbf{M}$, the step of (17) is necessary. This can be due to the fact that with a full eigenvalue analysis, the difference between (25) and (26) is at the level of machine precision. Hence, the contribution from the additional nullspace is negligible. However, this is not true with a partial eigenvalue analysis of $\mathbf{M}$ for obtaining $\mathbf{V}_h$ modes only.

C. Further Simplification of the Proposed Method

With the step of (17) added for removing the contribution from the additional nullspace, we found that the $\mathbf{V}_h\mathbf{V}_h^T\mathbf{T}u^n$ term can be omitted in (16). In other words, one treatment of (17) is sufficient. This is because in the implementation of (16), for efficient computation, instead of computing a new updated matrix $\mathbf{T}^{-1}\mathbf{S}(\mathbf{I} - \mathbf{V}_h\mathbf{V}_h^T\mathbf{T})$, we compute $(\mathbf{I} - \mathbf{V}_h\mathbf{V}_h^T\mathbf{T})u^n$ first, and then multiply it with $\mathbf{T}^{-1}\mathbf{S}$. The computation of $(\mathbf{I} - \mathbf{V}_h\mathbf{V}_h^T\mathbf{T})u^n$ essentially removes the $\mathbf{V}_h$-component from the field solutionu^n. Since this has already been done in the previous time step via (17), we do not have to do it again unless (17) does not clean up $\mathbf{V}_h$-component completely due to numerical round-off error. However, in this case, (17) can also be repeated a few times to make the field solution clean of unstable modes.

Without $\mathbf{V}_h\mathbf{V}_h^T\mathbf{T}$ term in (16), apparently, the numerical system would contain unstable modes. However, (17) forces the field solution u to be in the stable space $\mathbf{V}_s$ at each time step, and hence (16) is nothing but

$$\mathbf{V}_s {y_s}^{n+1} = 2\mathbf{V}_s {y_s}^{n} - \Delta t^2\mathbf{T}^{-1}\mathbf{S}\mathbf{V}_s {y_s}^{n} - \mathbf{V}_s {y_s}^{n-1} + \Delta t^2\mathbf{T}^{-1}\dot{I}^n.$$

Since $\mathbf{T}^{-1}\mathbf{S}\mathbf{V}_s = \mathbf{M}\mathbf{V}_s = \mathbf{V}_s\Lambda_s$, the term associated with $\mathbf{S}$ in the above is actually $\mathbf{V}_s\Lambda_s$, and hence the space of stable modes only.

The aforementioned simplification is attributed to the special design of (17) that utilizes the $\mathbf{T}$-orthogonality of the eigenvectors to make $u^n = \mathbf{V}_s {y_s}^n$, and hence when multiplied by $\mathbf{M}$, only the $\mathbf{V}_s$-component of the system matrix $\mathbf{M}$ is left.

It is also worth mentioning that the proposed method can also be leveraged in implicit time-domain methods to improve their accuracy and late-time instability. Instead of performing an implicit simulation of the original (1), one can perform an implicit simulation on the updated numerical system shown in (15). Since the unstable eigenmodes have been deducted from (15), what is left in the numerical system can all be accurately simulated by the given time step, the accuracy and late-time instability of an implicit method can be improved as well.

D. Finding Unstable Modes $\mathbf{V}_h$

$\mathbf{V}_h$ modes have the largest eigenvalues of (8) since they satisfy (9). This fact together with the sparsity of the TDFEM matrices can be utilized to find $\mathbf{V}_h$ efficiently. In this work, we use the implicitly restarted Arnoldi algorithm to find $\mathbf{V}_h$ [15], [17]. For finding k largest eigenvalues and their eigenvectors, the computation of this algorithm is mainly $O(k)$ sparse matrix-vector multiplications, and the orthogonalization of the obtained O(k) vectors. The computational complexity is $O(k^2N)$, thus efficient as compared to a traditional full eigenvalue analysis whose complexity is $O(N^3)$.

It is worth mentioning that if using the Arnoldi algorithm to find the stable eigenmodes instead of the unstable ones, the resultant computation is not efficient and robust. First of all, the stable modes have the smallest eigenvalues of the system matrix, while an Arnoldi solver converges to the largest eigenvalues first. If we work on the inverse of the original system matrix to transform the smallest eigenvalues to the largest ones, the sparsity of the original matrix is lost, and the computation becomes much more expensive. If we still work on the original matrix, it takes many more than k steps to find k smallest eigenvalues. Furthermore, the eigenvalue problem (8) has a large nullspace whose eigenvalues are zero, to find some completely is numerically difficult. In contrast, the algorithm developed in [11] is particularly robust and efficient for finding the stable eigenmodes. However, for finding the largest eigenvalues of a sparse numerical system, the Arnoldi solver is efficient and reliable for use.

IV. Proposed Method for Lossy Problems

Different from a lossless problem, a lossy problem is governed by a quadratic eigenvalue problem shown in (6). The resulting eigenvalues and eigenvectors are also complex valued. In this section, we will first perform a theoretical analysis to understand the nature of the problem, and then proceed to the proposed method, followed by a proof on its correctness. We also present another explicit marching scheme, and discuss a scaling technique.

A. Theoretical Analysis

Equation (1) can be transformed to the following first-order partial differential equation in time without any approximation:

$$\begin{bmatrix}\mathbf{R} & \mathbf{T}\\ \mathbf{T} & \mathbf{0}\end{bmatrix}\frac{d}{dt}\begin{Bmatrix}u\\ \dot{u}\end{Bmatrix} + \begin{bmatrix}\mathbf{S} & 0\\ 0 & -\mathbf{T}\end{bmatrix}\begin{Bmatrix}u\\ \dot{u}\end{Bmatrix} = \begin{Bmatrix}\dot{I}\\ 0\end{Bmatrix} \tag{30}$$

which can be written in short as

$$\frac{d}{dt}\tilde{u} - \mathbf{M}\tilde{u} = \tilde{b} \tag{31}$$

where $\tilde{u} = [u\ \ \dot{u}]^T$, $\tilde{b} = [0\ \ \mathbf{T}^{-1}\dot{I}]^T$, $\mathbf{M}$ is

$$\mathbf{M} = \mathbf{A}^{-1}\mathbf{B} \tag{32}$$

with

$$\mathbf{A} = \begin{bmatrix} \mathbf{R} & \mathbf{T} \\ \mathbf{T} & \mathbf{0} \end{bmatrix} \quad \mathbf{B} = \begin{bmatrix} -\mathbf{S} & 0 \\ 0 & \mathbf{T} \end{bmatrix}. \tag{33}$$

Using block matrix inversion formula, the $\mathbf{M}$ can be analytically found as

$$\mathbf{M} = \begin{bmatrix} 0 & \mathbf{I} \\ -\mathbf{T}^{-1}\mathbf{S} & -\mathbf{T}^{-1}\mathbf{R} \end{bmatrix}. \tag{34}$$

The solution of $\tilde{u}$, whose upper part is the original field solution of (1), is governed by the following generalized eigenvalue problem:

$$\mathbf{MV} = \mathbf{V}\mathbf{\Lambda} \tag{35}$$

in which $\mathbf{\Lambda}$ denotes a diagonal matrix whose entries are eigenvalues λ, and $\mathbf{V}$ is the eigenvector matrix which is $\mathbf{V} = [\mathbf{V}_s \ \mathbf{V}_h]$.

The original quadratic eigenvalue problem of (6) is equivalent to the generalized eigenvalue problem shown in (35). To see this point clearly, (6) can be rewritten as

$$\begin{bmatrix} -\mathbf{S} & 0 \\ 0 & \mathbf{T} \end{bmatrix} \begin{Bmatrix} v \\ \lambda v \end{Bmatrix} = \lambda \begin{bmatrix} \mathbf{R} & \mathbf{T} \\ \mathbf{T} & \mathbf{0} \end{bmatrix} \begin{Bmatrix} v \\ \lambda v \end{Bmatrix} \tag{36}$$

and in short as

$$\mathbf{B}V = \lambda \mathbf{A}V \tag{37}$$

and hence the same as (35) since $\mathbf{A}^{-1}\mathbf{B} = \mathbf{M}$, as given in (31). As a result, the eigenvalues of the generalized eigenvalue problem (37) are the same as those of (6), and the eignvectors of (37) in their upper half are the eigenvectors of (6).

If a forward-difference based explicit time marching is performed on (31), we can find the eigenmodes, whose nonzero eigenvalues λ_i satisfy the following condition, can be stably simulated by the given time step:

$$\frac{|\lambda_i|^2}{|\mathrm{Re}(\lambda_i)|} < \frac{2}{\Delta t} \tag{38}$$

a detailed derivation of which can be found in Appendix. In addition, the eigenmodes whose eigenvalues are zero can always be stably simulated. Given a time step, $\mathbf{V}_s$ is thus made of these eigenmodes that can be stably simulated by the given time step.

Since $\mathbf{V}_h$-modes and $\mathbf{V}_s$-modes have different eigenvalues, and both $\boldsymbol{A}$ and $\boldsymbol{B}$ of (37) are symmetric, $\mathbf{V}_h$and $\mathbf{V}_s$satisfy the following property:

$$\mathbf{V}_s^T \mathbf{A} \mathbf{V}_h = \mathbf{V}_h^T \mathbf{A} \mathbf{V}_s = 0 \tag{39}$$

To prove, consider two eigenpairs $(\lambda_1, v_1)$and $(\lambda_2, v_2)$of (37), whose eigenvalues are different. We have

$$\mathbf{B}v_1 = \lambda_1 \mathbf{A}v_1 \quad \mathbf{B}v_2 = \lambda_2 \mathbf{A}v_2$$

from which we obtain

$${v_2}^T \mathbf{B}v_1 = \lambda_1 {v_2}^T \mathbf{A}v_1 \quad {v_1}^T \mathbf{B}v_2 = \lambda_2 {v_1}^T \mathbf{A}v_2.$$

Taking the transpose of the first equation, and subtracting the second from it, since $\mathbf{A}$ and $\mathbf{B}$ are symmetric, and the two eigenvalues are different, we have ${v_2}^T \mathbf{A}v_1 = {v_2}^T \mathbf{B}v_1 = 0$.

As a result, we can deduce

$$\mathbf{V}^T \mathbf{A} \mathbf{V} = \begin{bmatrix} \mathbf{V}_s^T \\ \mathbf{V}_h^T \end{bmatrix} \mathbf{A} \begin{bmatrix} \mathbf{V}_s \ \mathbf{V}_h \end{bmatrix} = \begin{bmatrix} \mathbf{A}_t & 0 \\ 0 & \mathbf{D}_h \end{bmatrix} \tag{40}$$

where

$$\begin{aligned} \mathbf{A}_t &= \mathbf{V}_s^T \mathbf{A} \mathbf{V}_s \\ \mathbf{D}_h &= \mathbf{V}_h^T \mathbf{A} \mathbf{V}_h. \end{aligned} \tag{41}$$

Following the same proof as the above, $\mathbf{D}_\mathrm{h}$ is also a diagonal matrix since the eigenvalues of $\mathbf{V}_h$ are nonzero, and the nonzero eigenvalues of (37), in general, are not identical. In the rare case where a few eigenvalues are the same, $\mathrm{D_h}$ is block diagonal with a very small block size being the number of repeated eigenvalues. Hence, its inversion is trivial.

B. Method

Given an arbitrary time step, to overcome the instability of an explicit marching, we simply update the original system of (31) to a new system of equations as the following:

$$\frac{d}{dt}\tilde{u} - \mathbf{M}\left(\mathbf{I} - \mathbf{V}_h \mathbf{D}_h^{-1} \mathbf{V}_h^T \mathbf{A}\right) \tilde{u} = \tilde{b} \tag{42}$$

where $\mathbf{M}$ is changed to a new system matrix $\mathbf{M}(\mathbf{I} - \mathbf{V}_h \mathbf{D}_h^{-1} \mathbf{V}_h^T \mathbf{A})$. We then perform a forward-difference based explicit time marching of (42) as the following:

$$\tilde{\tilde{u}}^{n+1} = \tilde{u}^n - \Delta t \mathbf{M}\left(\mathbf{I} - \mathbf{V}_h \mathbf{D}_h^{-1} \mathbf{V}_h^T \mathbf{A}\right) \tilde{u}^n + \Delta t \tilde{b}^n \tag{43}$$

where the only computation additional to the conventional TDFEM is the evaluation of $\mathbf{V}_h \mathbf{D}_h^{-1} \mathbf{V}_h^T \mathbf{A} \tilde{u}^n$. This term can be efficiently computed by a sequence of matrix-vector multiplications from right to left, the computational cost of which is $O(kN)$, where k is the number of columns in $\mathbf{V}_h$, i.e., the number of unstable modes.

Similar to the lossless cases, after the field solution is obtained via (43) at each time step, we add the following treatment:

$$\tilde{u}^{n+1} = \tilde{\tilde{u}}^{n+1} - \mathbf{V}_h \mathbf{D}_h^{-1} \mathbf{V}_h^T \mathbf{A} \tilde{\tilde{u}}^{n+1}. \tag{44}$$

Since the step of (44) is performed at each step, the $\mathbf{V}_h \mathbf{D}_h^{-1} \mathbf{V}_h^T \mathbf{A} \tilde{u}^n$ in (43) can be saved.

C. How it Works?

Like the lossless cases, the above modification shown in (42) changes the original system involving both unstable and stable modes to a system of stable modes only. To prove, now, the new system matrix

$$\mathbf{M}_{\mathrm{new}} = \mathbf{M}\left(\mathbf{I} - \mathbf{V}_h \mathbf{D}_h^{-1} \mathbf{V}_h^T \mathbf{A}\right). \tag{45}$$

We can show it only contains the stable eigenmodes of the original system matrix $\boldsymbol{M}$**,** and an additional nullspace as the following.

From (40), we obtain

$$\mathbf{V}^{-1} = \begin{bmatrix} \mathbf{A}_t^{-1} & 0 \\ 0 & \mathbf{D}_h^{-1} \end{bmatrix} \mathbf{V}^T \mathbf{A}. \tag{46}$$

Hence, the original $\mathbf{M}$ can be rewritten as

$$\begin{aligned}\mathbf{M} = \mathbf{V}\Lambda\mathbf{V}^{-1} &= [\mathbf{V}_s\ \mathbf{V}_h][\Lambda]\begin{bmatrix}\mathbf{A}_t^{-1} & 0\\ 0 & \mathbf{D}_h^{-1}\end{bmatrix}[\mathbf{V}_s\ \mathbf{V}_h]^T\mathbf{A}\\ &= [\mathbf{V}_s\ \mathbf{V}_h]\begin{bmatrix}\Lambda_s & 0\\ 0 & \Lambda_h\end{bmatrix}\begin{bmatrix}\mathbf{A}_t^{-1} & 0\\ 0 & \mathbf{D}_h^{-1}\end{bmatrix}\\ &\quad\times[\mathbf{V}_s\ \mathbf{V}_h]^T\mathbf{A}\\ &= \mathbf{V}_s\Lambda_s\mathbf{A}_t^{-1}\mathbf{V}_s^T\mathbf{A} + \mathbf{V}_h\Lambda_h\mathbf{D}_h^{-1}\mathbf{V}_h^T\mathbf{A}\\ &= \mathbf{V}_s\Lambda_s\mathbf{A}_t^{-1}\mathbf{V}_s^T\mathbf{A} + \mathbf{M}\mathbf{V}_h\mathbf{D}_h^{-1}\mathbf{V}_h^T\mathbf{A} \quad (47)\end{aligned}$$

where in the last step, we utilize the fact that $\mathbf{M}\mathbf{V}_h = \mathbf{V}_h\Lambda_h$. Therefore, the modified system matrix is nothing but

$$\mathbf{M}_{\text{new}} = \mathbf{V}_s\Lambda_s\mathbf{A}_t^{-1}\mathbf{V}_s^T\mathbf{A} \quad (48)$$

the $\mathbf{V}_s$-component of $\mathbf{M}$. Multiplying both sides of the above by $\mathbf{V}_s$, recognizing $\mathbf{V}_s^T\mathbf{A}\mathbf{V}_s = \mathbf{A}_t$ as can be seen from (41), we obtain

$$\mathbf{M}_{\text{new}}\mathbf{V}_s = \mathbf{V}_s\mathbf{\Lambda}_s. \quad (49)$$

Hence, $(\mathbf{\Lambda}_s,\ \mathbf{V}_s)$ is the eigenvalue solution of $\mathbf{M}_{\text{new}}$. Therefore, the new system matrix contains the stable eigenmodes only. As a result, an explicit marching of (43) is absolutely stable for the given time step no matter how large it is.

Similar to the lossless cases, since the rank of (48), and hence $\mathbf{M}_{\text{new}}$, is the number of stable eigenmodes k_s, while the matrix size of (48) is 2*N*, the $\mathbf{M}_{\text{new}}$ is a low-rank matrix with (2*N*-k_s) additional zero eigenvalues. The eigenvectors corresponding to these zero eigenvalues form a nullspace that is not present in the original system matrix $\mathbf{M}$, which makes the field solution incorrect. Therefore, like the lossless cases, after the field solution is obtained via (43) at each time step, we add the treatment shown in (44) to remove the contribution from the additional nullspace, making the field solution correct. To explain, the $\tilde{u}^{n+1}$ again has a form of (28), since $\mathbf{V}_h^T\mathbf{A}\mathbf{V}_s = 0$, and $\mathbf{V}_h^T\mathbf{A}\mathbf{V}_h = \mathbf{D}_h$, the $\mathbf{V}_h\mathbf{D}_h^{-1}\mathbf{V}_h^T\mathbf{A}\tilde{u}^{n+1}$ is nothing but the component of $\tilde{u}^{n+1}$ contributed by the additional nullspace. By deducting it from $\tilde{u}^{n+1}$, we obtain the $\mathbf{V}_s$-component only.

D. Another Explicit Time Marching Scheme Based on Central Difference

For a general lossy problem discretized into a second-order system shown in (1), we can directly simulate it with a central-difference-based explicit time marching. The scheme described above transforms (1) to a first-order system, and simulates the resultant with a forward-difference-based explicit marching. Readers who have experiences with the two explicit time marching schemes may have realized that the two schemes have a different requirement on time step for stability. When there is a conductor loss, the time step required by a forward-difference explicit marching can be much smaller than that of the central-difference-based explicit marching. Although in the proposed new method, we remove the unstable modes from the numerical system according to time step, and hence allowing for the forward-difference scheme to use any large time step. However, from an accuracy point of view, for simulating the same set of eigenmodes kept in the numerical system, the time step required by a forward-difference explicit marching for stably simulating these modes is smaller than that of a central-difference-based explicit marching. In this subsection, we analyze this problem and present a central-difference-based explicit marching scheme for simulating the lossy problems with unconditional stability.

Using a central-difference-based explicit marching of (1), the time step required for stably simulating an eigenmode of λ_i eigenvalue satisfies the following condition [12], as also shown in (10):

$$\Delta t \le \frac{2}{\sqrt{|\lambda_{i1}\lambda_{i2}|}}. \quad (50)$$

However, using a forward-difference scheme, as shown in (38), the time step needs to satisfy

$$\Delta t \le \frac{2|\text{Re}(\lambda_i)|}{|\lambda_i|^2}. \quad (51)$$

For an eigenvalue pair having identical negative eigenvalues, (51) is the same as (50). For complex conjugate eigenvalues, from (5), we can find

$$\lambda_i = \frac{-b_i \pm \sqrt{{b_i}^2 - 4c_i}}{2} \quad (52)$$

where $b_i = V_i^H\mathbf{R}V_i/V_i^H\mathbf{T}V_i$, $c_i = V_i^H\mathbf{S}V_i/V_i^H\mathbf{T}V_i$ and both are greater than zero. Since for complex conjugate eigenvalues, ${b_i}^2 < 4c_i$, and $|\lambda_i| = \sqrt{c_i}$, we have $|\text{Re}(\lambda_i)| = b_i/2 < |\lambda_i|$. Hence, the time step of (51) is smaller than that required in (50), because $\Delta t \le \frac{2|\text{Re}(\lambda_i)|}{|\lambda_i|^2} < \frac{2}{|\lambda_i|}$.

We propose to perform a leap-frog-based time marching of the first-order system of (31). This will yield the same central-difference-based time marching of the original second-order system (1), and hence resulting in a time step of (50) for stability, which is larger than that allowed by the forward-difference-based time marching for simulating the same eigenmode. To explain, we can write (31) in full as

$$\frac{d}{dt}\begin{Bmatrix}u\\ w\end{Bmatrix} - \begin{bmatrix}0 & \mathbf{I}\\ -\mathbf{T}^{-1}\mathbf{S} & -\mathbf{T}^{-1}\mathbf{R}\end{bmatrix}\begin{Bmatrix}u\\ w\end{Bmatrix} = \begin{Bmatrix}0\\ \tilde{b}_2\end{Bmatrix} \quad (53)$$

where $w = \dot{u}$, which is also an unknown to be solved together with the field solution *u*, and $\tilde{b}_2$ is the lower half of vector $\tilde{b}$. Using a leap-frog-based time marching, the above double-sized first-order system can be marched on in time as follows:

$$\begin{aligned}u^n - u^{n-1} &= \Delta t w^{n-\frac{1}{2}}\\ w^{n+\frac{1}{2}} - w^{n-\frac{1}{2}} + \Delta t\mathbf{T}^{-1}\mathbf{S}u^n + \Delta t\mathbf{T}^{-1}\mathbf{R}&\frac{w^{n+\frac{1}{2}} + w^{n-\frac{1}{2}}}{2}\\ &= \Delta t\tilde{b}_2^n \quad (54)\end{aligned}$$

which can be rearranged to solve *u* and *w* at the most advanced time step as

$$u^n = u^{n-1} + \Delta t w^{n-\frac{1}{2}} \quad (55)$$

$$\begin{aligned}\left(\mathbf{I} + 0.5\Delta t\mathbf{T}^{-1}\mathbf{R}\right)w^{n+\frac{1}{2}} &= \left(\mathbf{I} - 0.5\Delta t\mathbf{T}^{-1}\mathbf{R}\right)w^{n-\frac{1}{2}}\\ &\quad - \Delta t\mathbf{T}^{-1}\mathbf{S}u^n + \Delta t\tilde{b}_2^n \quad (56)\end{aligned}$$

The above is equivalent to a central-difference-based discretization of (1). This can be readily proved as follows. Writing (55) for the n+1-th step, we obtain

$$u^{n+1} = u^n + \Delta t w^{n+\frac{1}{2}}. \quad (57)$$

Multiplying both sides by $(\mathbf{I}+0.5\Delta t\mathbf{T}^{-1}\mathbf{R})$, we have

$$\left(\mathbf{I}+0.5\Delta t\mathbf{T}^{-1}\mathbf{R}\right)u^{n+1} = \left(\mathbf{I}+0.5\Delta t\mathbf{T}^{-1}\mathbf{R}\right)u^{n} + \Delta t\left(\mathbf{I}+0.5\Delta t\mathbf{T}^{-1}\mathbf{R}\right)w^{n+\frac{1}{2}}. \tag{58}$$

Multiplying (55) by $(\mathbf{I}-0.5\Delta t\mathbf{T}^{-1}\mathbf{R})$on both sides, we obtain

$$\left(\mathbf{I}-0.5\Delta t\mathbf{T}^{-1}\mathbf{R}\right)u^{n} = \left(\mathbf{I}-0.5\Delta t\mathbf{T}^{-1}\mathbf{R}\right)u^{n-1} + \Delta t\left(\mathbf{I}-0.5\Delta t\mathbf{T}^{-1}\mathbf{R}\right)w^{n-\frac{1}{2}}. \tag{59}$$

Subtracting (59) from (58), and substituting (56), we have

$$(\mathbf{I}+0.5\Delta t\mathbf{T}^{-1}\mathbf{R})u^{n+1} = 2u^{n}-(\mathbf{I}-0.5\Delta t\mathbf{T}^{-1}\mathbf{R})u^{n-1} - \Delta t^{2}\mathbf{T}^{-1}\mathbf{S}u^{n}+\Delta t^{2}\mathbf{T}^{-1}\dot{I}^{n} \tag{60}$$

which is the same as a central-difference-based discretization of (1). Hence, by performing a time marching of the first-order system (31) in a leap-frog-based way shown in (55) and (56), the time step required for stably simulating an eigenmode is same as that of a central-difference-based time marching of the second-order system.

With the unstable modes $\mathbf{V}_h$ satisfying (10) found from (37), to make the above leap-frog scheme shown in (55–56) stable for any time step, what we only need to do is as follows. After (55), we form vector $\tilde{u}=[u^n w^{n-\frac{1}{2}}]^T$, and deduct the unstable modes from it by updating it to be $\tilde{u}=(\mathbf{I}-\mathbf{V}_h\mathbf{D}_h^{-1}\mathbf{V}_h^T\mathbf{A})\tilde{u}$. u^n is then taken as the upper half of $\tilde{u}$ to be free of unstable modes, and used in (56) to compute $w^{n+\frac{1}{2}}$. After the computation of (56) for obtaining $w^{n+\frac{1}{2}}$, we form $\tilde{u}=[u^n w^{n+\frac{1}{2}}]^T$, update it to be $\tilde{u}=(\mathbf{I}-\mathbf{V}_h\mathbf{D}_h^{-1}\mathbf{V}_h^T\mathbf{A})\tilde{u}$ so that the unstable modes are removed. u^n is then updated to be the upper half of $\tilde{u}$, while $w^{n+\frac{1}{2}}$ is updated to be the lower half of $\tilde{u}$. We then continue to next time step. The entire procedure is summarized as the following:

$$\begin{aligned}
&(1)\quad u^n = u^{n-1}+\Delta t w^{n-\frac{1}{2}}\\
&(2)\quad \tilde{u}=\left[u^n w^{n-\frac{1}{2}}\right]^T\\
&\qquad \tilde{u}=(\mathbf{I}-\mathbf{V}_h\mathbf{D}_h^{-1}\mathbf{V}_h^T\mathbf{A})\tilde{u}\\
&\qquad u^n = \tilde{u}(1:N)\\
&(3)\quad (\mathbf{I}+0.5\Delta t\mathbf{T}^{-1}\mathbf{R})w^{n+\frac{1}{2}}\\
&\qquad = (\mathbf{I}-0.5\Delta t\mathbf{T}^{-1}\mathbf{R})w^{n-\frac{1}{2}}-\Delta t\mathbf{T}^{-1}\mathbf{S}u^n+\Delta t\tilde{b}_2^n\\
&(4)\quad \tilde{u}=\left[u^n w^{n+\frac{1}{2}}\right]^T\\
&\qquad \tilde{u} = (\mathbf{I}-\mathbf{V}_h\mathbf{D}_h^{-1}\mathbf{V}_h^T\mathbf{A})\tilde{u}\\
&\qquad u^n = \tilde{u}(1:N)\\
&\qquad w^{n+\frac{1}{2}} = \tilde{u}(N+1:2N)
\end{aligned} \tag{61}$$

where steps (1) and (3) are the same as the original (55) and (56), but steps (2) and (4) are added to ensure the unstable modes are removed from the numerical system at each time step.

E. Scaling

During the study of this paper, we found that when **T**, **S,** and **R** are very different in their norm, the solution of the generalized eigenvalue problem (37), which is equivalent to the original quadratic eigenvalue problem (6), may have a poor accuracy in numerical computation. This is especially true when the problems being simulated involve conductor loss and/or multiple scales. We hence adopt a scaling technique introduced in [17] to achieve good accuracy in the solution of (37) for finding the unstable modes. Based on this scaling technique, the matrix **T**, **S,** and **R** in (36) are, respectively, scaled to

$$\tilde{\mathbf{T}}=\alpha^2\beta\mathbf{T}\quad \tilde{\mathbf{S}}=\beta\mathbf{S}\quad \tilde{\mathbf{R}}=\alpha\beta\mathbf{R} \tag{62}$$

where

$$\begin{aligned}
&\alpha=\sqrt{\gamma_0/\gamma_2}\\
&\beta = 2/\left(\gamma_0+\gamma_1\sqrt{\gamma_0/\gamma_2}\right)\\
&\gamma_2=||\mathbf{T}||_2\quad \gamma_1=||\mathbf{R}||_2\quad \gamma_0=||\mathbf{S}||_2.
\end{aligned} \tag{63}$$

Correspondingly, the first-order double-sized system (30) is updated as the following:

$$\frac{1}{\alpha}\begin{bmatrix}\tilde{\mathbf{R}} & \tilde{\mathbf{T}}\\ \tilde{\mathbf{T}} & \mathbf{0}\end{bmatrix}\frac{d}{dt}\begin{Bmatrix}u\\ \alpha^{-1}\dot{u}\end{Bmatrix}+\begin{bmatrix}\tilde{\mathbf{S}} & 0\\ 0 & -\tilde{\mathbf{T}}\end{bmatrix}\begin{Bmatrix}u\\ \alpha^{-1}\dot{u}\end{Bmatrix}=\begin{Bmatrix}\beta\dot{I}\\ 0\end{Bmatrix} \tag{64}$$

which can be compactly written as

$$\frac{d}{dt}\tilde{u}'-\tilde{\mathbf{M}}\tilde{u}'=\tilde{b}' \tag{65}$$

where

$$\begin{aligned}
&\tilde{u}'=\begin{bmatrix}u\\ \alpha^{-1}\dot{u}\end{bmatrix}\quad \tilde{\mathbf{M}}=\tilde{\mathbf{A}}^{-1}\tilde{\mathbf{B}},\\
&\tilde{\mathbf{A}}=\frac{1}{\alpha}\begin{bmatrix}\tilde{\mathbf{R}} & \tilde{\mathbf{T}}\\ \tilde{\mathbf{T}} & \mathbf{0}\end{bmatrix}\quad \tilde{\mathbf{B}}=\begin{bmatrix}-\tilde{\mathbf{S}} & 0\\ 0 & \tilde{\mathbf{T}}\end{bmatrix}.
\end{aligned} \tag{66}$$

In this paper, all the lossy examples are simulated with the above scaled numerical system (65) instead of the original unscaled system (31). As can be seen from $\tilde{u}'$ in (66), the upper half of the solution vector obtained from (65) is the same as that of (31). The unstable modes are hence found from the scaled system matrix $\tilde{\mathbf{M}}$, the accuracy of which is much improved.

V. Numerical Results

In this section, we first demonstrate the unconditional stability of the proposed explicit time-domain method with an example having an analytical solution. We then simulate a suite of lossless and lossy examples to validate the accuracy, efficiency, and stability of the proposed method. The conventional TDFEM used for comparison employs a central-difference-based explicit time-marching. The explicit and unconditionally stable TDFEM recently developed in [11] is also involved for comparison. The computer used has an Intel i5 5300U 2.30 GHz processor, unless specified specifically.

All the examples simulated here involve fine physical features smaller than working wavelengths. As a result, the time step dictated by space step for stability is smaller than that required by accuracy. Hence, they represent those problems where

the time step issue need to be overcome for computational efficiency. For the fine features, multiple scenarios are considered: the entire structure is fine as compared to working wavelengths but we cannot ignore the entire structure to study its interior characteristics; a part of the entire structure is fine but cannot be ignored since the resultant solution would be very different; and a multiscale structure. For the first scenario, all the modes are unstable modes except for the nullspace modes (dc modes). We show that even for such a scenario, the proposed method can have a significant speedup because the time step is increased significantly all the way up to that permitted by accuracy.

A. *Examination of Unconditional Stability*

We first examine the unconditional stability of the proposed method with a parallel-plate example that has an analytical solution. The length, width, and height of the structure are 900, 6, and 1 μm, respectively. The input source is a Gaussian derivative pulse of $I(t) = 2(t - t_0)\exp(-(t - t_0)^2/\tau^2)$ with $\tau = 0.2$ s and $t_0 = 4\tau$. The space step size is 100, 1.5, and 0.125 μm, respectively along the length, width, and height direction. This discretization results in 405 $\mathbf{E}_x$ unknowns, 360 $\mathbf{E}_y$ unknowns, and 400 $\mathbf{E}_z$ unknowns. Excluding 170 unknowns that are on the top and bottom PEC surfaces, the total number of unknowns is 995. Despite the low-frequency input spectrum, due to the small space step, conventional TDFEM has to use a time step as small as $\Delta t = 2.5 \times 10^{-16}$ s to ensure the stability of a time-domain simulation. In contrast, the time step required by accuracy is at the level of 0.01 s. Hence, there exists a more than thirteen-orders-of-magnitude difference between the time step restricted by space step for stability and the time step determined by accuracy.

The proposed explicit method is able to use the time step solely determined by accuracy to obtain stable and accurate results. As shown in Fig. 1(a), the voltages simulated by the proposed method with a time step as large as 0.001 and 0.01 s are in excellent agreement with the analytical solutions. The number of removed unstable modes, whose eigenvalues are greater than $2/\Delta t$, is 644 in this example out of 995 total number of eigenmodes. The 995 is also the total number of electric field unknowns in this example. In Fig. 1(b), we plot the result obtained from a backward-difference-based implicit method using 0.01 s as the time step. As can be seen, the result is completely wrong, which could be attributed to the much enlarged time step. In Fig. 1(c), with the same time step, we simulate the example to late time using the proposed method. The result is shown to be stable and accurate.

An unconditionally stable method should also permit the use of an arbitrarily large time step without becoming unstable. If infinity is the time step required by accuracy, for example, in the case of simulating an extremely low frequency, an unconditionally stable method should also be able use this time step to generate accurate results. This is true in the proposed method. In fact, in this example, after the 644 unstable modes are removed, the rest of the 351 modes are all nullspace modes whose eigenvalues are zero. We hence can use an infinitely large time step to simulate them stably.

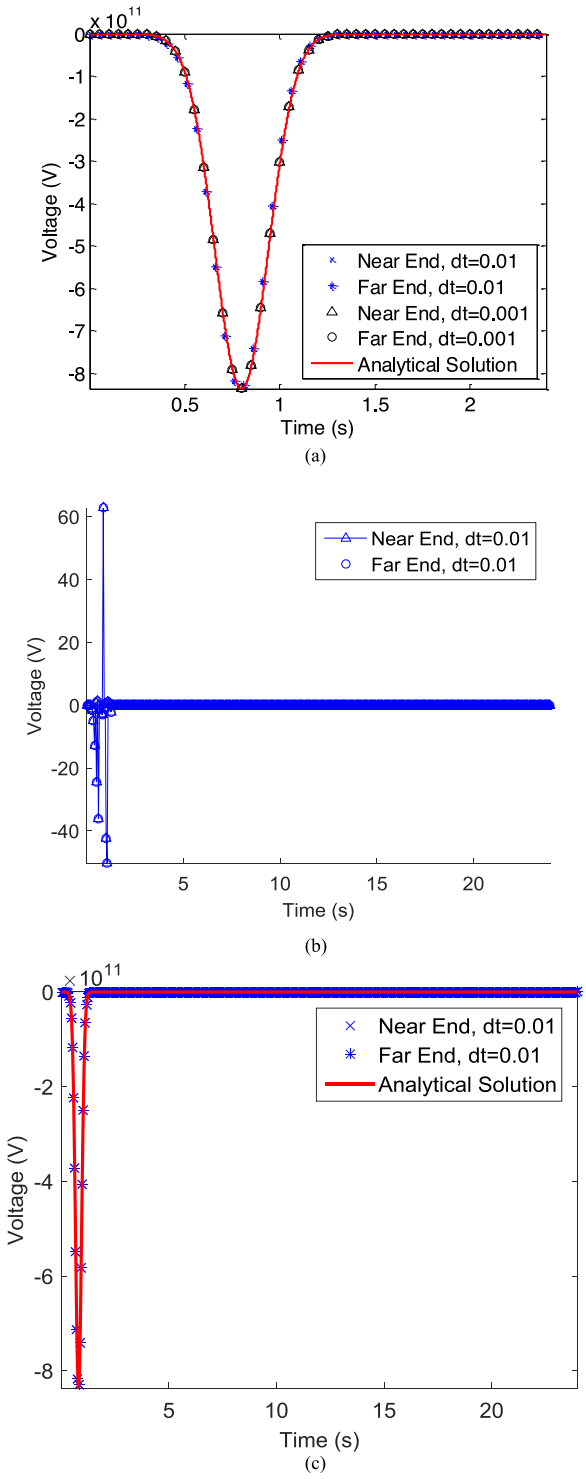

Fig. 1. (a) Demonstration of unconditional stability of the proposed method with an arbitrarily large time step. (b) Simulation result from an implicit method. (c) Late-time simulation result of the proposed method.

Notice that when different time steps are used, we do not need to recompute the unstable modes that have already been computed. If a larger time step is used, we add more unstable modes; if a smaller one is used, we select from the computed unstable modes whose eigenvalues satisfy (9) or (10).

B. Demonstration of Accuracy, Efficiency, and Stability

1) Millimeter-Level Inhomogeneous Lossless Waveguide: We consider an mm-level parallel-plate waveguide where fine features coexist with regular features. The length, width, and height of the structure are 120, 4.04, and 3.192 mm, respectively. Along the width, it is discretized into 11 segments, with the center one being 0.04-mm wide while the rest are 0.4-mm wide. The 0.04 mm fine discretization is used to capture a thin film whose dielectric constant is as high as 5000. This often arises from the passivation/barrier layer in a device manufacturing process. Along the length, a uniform step size of 10 mm is used; and along the height, it is discretized into five cells with the minimum cell size being 0.316 mm. The dielectric constant elsewhere is 4. The number of unknowns in this example is 1928, with the number of cells along x-, y-, and z-direction being 12, 11, and 5, respectively. The input source is a Gaussian derivative pulse of $I(t) = 2(t - t_0)\exp(-(t - t_0)^2/\tau^2)$ with $\tau = 8 \times 10^{-9}$ s and $t_0 = 3\tau$. Due to the presence of the 0.04-mm thin layer, conventional TDFEM requires $\Delta t = 10^{-12}$ s for a stable simulation. In contrast, the proposed method is able to use a time step of $\Delta t = 1 \times 10^{-10}$ s determined by accuracy to generate accurate and stable results. The voltages simulated by the proposed method at the near end of the waveguide is plotted in Fig. 2(a), in comparison with the reference results generated by the conventional explicit TDFEM. Excellent agreement can be observed. We find the center layer, though thin, plays a critical role in the field solution, i.e., the field solution will be changed if we ignore the thin layer of high permittivity. This can be seen clearly from the voltage plotted in Fig. 2(b), where the high permittivity layer is removed.

The CPU time of the proposed method for explicit time marching is 29.9 s. The time used for finding the $\mathbf{V}_h$ modes is 4.27 s. On the contrary, the CPU time of the traditional explicit TDFEM is 127.14 s on the same computer.

2) Lossy On-chip Power Grid Structure: The second lossy example is a power grid structure with lossy conductors, as shown in Fig. 3. The red lines denote power rails and the green ones are ground rails. There is a vertical via connecting two metal rails wherever the two wires of same polarity cross each other. The top and bottom planes are set to be ground planes and the other four sides are left open. The permittivity is shown in Fig. 3(b) and (c), and the conductivity of the metal is 5.0×10^7 S/ m. The minimum space step along x-, y-, and z-direction is 0.4, 0.4, and 0.2 μm, respectively, resulting in 8, 6, and 7 number of cells. The number of unknowns in this example is 1101, and hence a total number of 2202 modes of (37). The current source is launched between one power rail and one ground rail in the lower metal layer, and it has a Gaussian derivative pulse with $\tau = 3 \times 10^{-9}$ s and $t_0 = 4\tau$. The voltage between the two rails is sampled. The time step used in the proposed method is 1×10^{-10} s solely determined by accuracy while the time step of the central difference based conventional TDFEM is 5×10^{-16} s. Based on the required time step of 1×10^{-10} s, 1628 unstable modes are deducted from the system matrix. In Fig. 4(a), the near end voltage of the proposed method in comparison with the reference data obtained from the traditional TDFEM solution is shown. Excellent agreement is observed. In Fig. 4(b), the entire solution error is plotted versus time, which again validates the accuracy of the proposed method at all points in the computational domain. The large error at the center is due to zero passing, and hence comparison with close to zero fields. The increased error at the early and late time is also due to the comparison with close to zero fields.

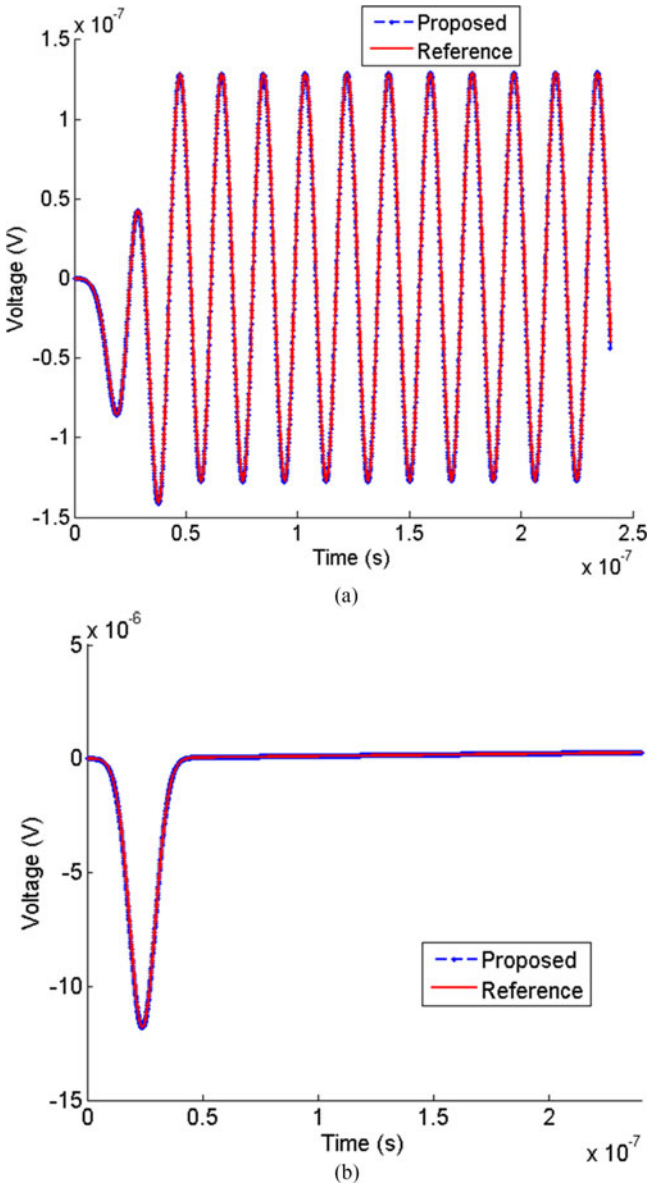

Fig. 2. Voltages of an mm-level inhomogeneous waveguide. (a) With a fine feature. (b) Without the fine feature.

The total time of the conventional TDFEM is 5.1668×10^3 s, while the CPU time of the proposed method is only 67.6576 s for finding unstable modes, and 12.1992 s for explicit time marching. Similar to the previous on-chip example, although most of the eigenmodes are unstable modes since the entire structure is small as compared to the working wavelength, the speedup of the proposed method is still significant. The leap-frog-based explicit marching described in Section IV-D is also used to simulate this example, which yields the same accurate results.

3) Lossy Multiscale Structure: In the previous two lossy examples, the time step from the forward-difference-based explicit

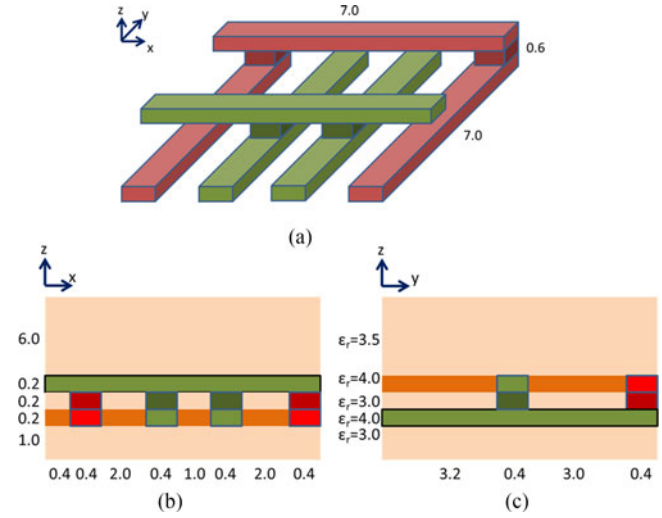

Fig. 3. Illustration of the on-chip bus structure (unit: μm). (a) Cross-sectional view (y–z plane). (b) Top view of the center metal layer.

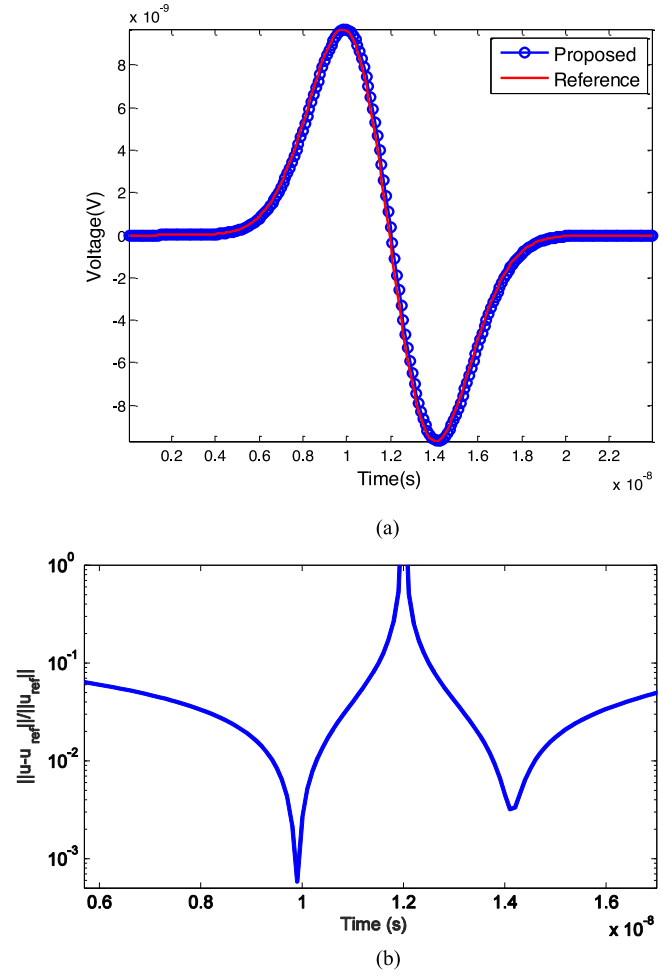

Fig. 4. Simulation of a lossy power grid structure. (a) Voltage. (b) Entire solution error versus time.

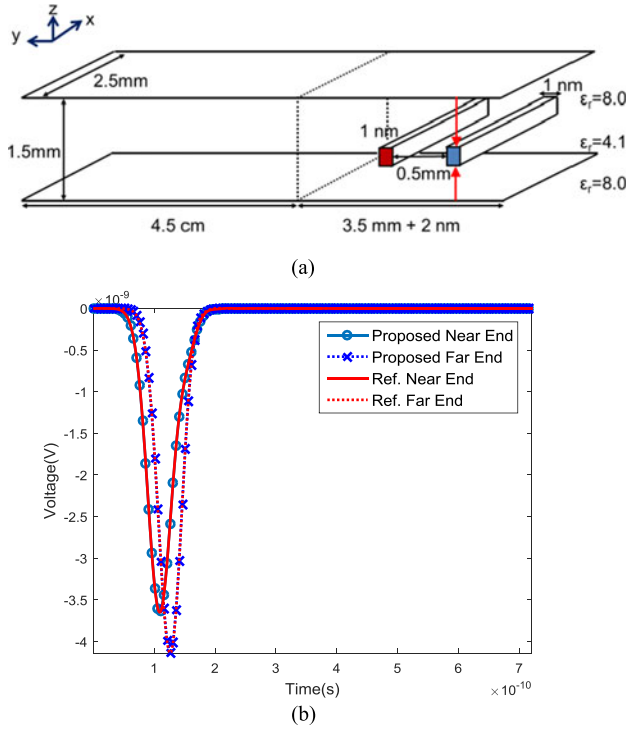

Fig. 5. Simulation of a lossy multiscale structure. (a) Geometry. (b) Voltages.

marching is the same as that of the central-difference-based one because the stable eigenmodes kept in the numerical system turn out to be nullspace modes only. In the last lossy example, we examine the validity of the proposed central-difference-based explicit time marching scheme described in Section IV-D in a problem where the time step resulting from a forward-difference explicit marching and that of a central-difference marching is very different.

The structure is illustrated in Fig. 5(a), where there are two thin wires of width 1 nm each, and the total width of the structure is the sum of 4.05 cm, 3.5 mm, and 2 nm. This problem setup resembles a multiscale integrated structure where board-level planes coexist with on-chip interconnects. In such a problem, regular structures (compared to wavelength) coexist with fine features, which is different from previous two on-chip examples where the entire structure is electrically small. For such a multiscale problem, unstable modes only occupy a portion of the entire number of modes; and the unstable mode number is proportional to the mesh elements used to discretize the fine features. There are three layers of 0.5-mm-thickness each, having the permittivities shown in Fig. 5(a). The space step is 0.5 mm except for the 1 nm-wide wires where a step size of 1 nm is used. The number of cells is 5,4500, and 3 along x-, y-, and z-direction, respectively. The number of unknowns in this example is 3628, and hence 7256 modes of (37). The input current sources are launched from the bottom and the top metal plate to the inner lossy conductor of conductivity 5.8×10^7 s/m. The sources have a Gaussian derivative pulse of $I(t) = 2(t - t_0)\exp(-(t - t_0)^2/\tau^2)$ with $\tau = 3 \times 10^{-11}$ s and $t_0 = 4\tau$. The time step used in the proposed method is 1×10^{-12} s solely determined by accuracy while the time step of the

central-difference-based conventional TDFEM is 3×10^{-15} s. Based on the required time step of 1×10^{-12} s, 130 eigenmodes are identified as unstable modes and removed from the numerical system based on (60). In this example, if a forward-difference explicit marching is used, the time step would have to be as small as 3×10^{-26} s for simulating the same set of stable modes kept in the numerical system. This is because many of them are complex conjugate eigenvalues, which render the time step resulting from (51) much smaller than that of (50).

The marching time of the conventional TDFEM is 1.9923 $\times 10^2$ s. In contrast, the marching time of the proposed leap-frog central-difference algorithm is 14.1493 s, and the CPU time spent on finding the unstable modes is only 2.1216 s. Again, very good agreement between the proposed method and the conventional TDFEM is observed as can be seen from the waveforms plotted in Fig. 5(b).

The structure is then further enlarged to result in a larger number of unknowns of 180 028, and hence 360 056 total number of modes of (37). To be specific, the left segment of 4.5 cm width of Fig. 5(a) is duplicated to the left to enlarge the width of the structure as well as the number of unknowns. For this large case, the conventional TDFEM takes more than 16 h to finish the entire explicit time marching, whereas the proposed explicit method only takes 125 min for explicit time marching, with less than 7 min spent on finding the unstable modes. Out of the 360 056 total number of modes, only 130 modes are unstable. This number is also the same as that obtained from the original structure. This is because the fine features remain the same when we enlarge the structure.

VI. Conclusion

In this paper, an alternative explicit and unconditionally stable TDFEM is developed for analyzing both lossless and general lossy problems. In this method, the source of instability is upfront deducted from the system matrix before performing explicit time marching. As a result, the explicit time marching is made absolutely stable for the given time step no matter how large it is. The accuracy of the proposed method is also theoretically guaranteed when the time step is chosen based on accuracy. The proposed method is convenient for implementation since it only requires a minor modification of the traditional explicit TDFEM method to eradicate the source of instability. The additional computation involved in the proposed method as compared with a traditional TDFEM is mainly the cost of finding unstable modes. Since the unstable modes have the largest eigenvalues of the sparse TDFEM system matrix, they can be found efficiently in $O(k^2N)$ complexity, where k is the number of unstable modes. In addition, these modes are frequency, time, and right hand side independent. Once found, they can be reused for different simulations, and also for different choices of time step.

The proposed new method complements the recently developed explicit and unconditionally stable TDFEM in [11]. When the fine features only occupy a small portion of the entire structure, the proposed method can be more advantageous to use as compared to [11], since the number of unstable modes is small whereas the number of stable modes is many. When the unstable mode number is large, the computational cost of finding these modes would become large. In this case, [11] can be more efficient for use. However, even in this case, one can still remove a certain number of unstable modes allowed by his computational resources, and thus immediately enlarging the time step. To be specific, if we sort the eigenvalues based on their magnitude from the largest λ_1 to the smallest λ_N, then by removing one largest eigenvalue, we enlarge the time step to $2/|\lambda_2|$; by removing 20 largest eigenvalues, we enlarge the time step to $2/|\lambda_{20}|$. So the number of unstable modes to remove is up to the user's choice, unlike [11], where all stable modes have to be found for an accurate solution. This is because in [11], the field solution is expanded into these stable modes, which are also physically important modes. If one mode is missing, the accuracy is affected. Here, there is a maximum number of unstable modes one can remove, which is determined by the time step required by accuracy. However, there is no minimum number of unstable modes one has to remove. One can find a few and remove only a few to enlarge the time step. In addition, the method of this work and [11] can also be combined for use to accentuate the advantages of both methods.

Appendix

Consider a first-order differential equation in time

$$\mathbf{A}\frac{d}{dt}\tilde{u} - \mathbf{B}\tilde{u} = \tilde{f}. \tag{A.1}$$

The governing eigenvalue problem is

$$\mathbf{BV} = \mathbf{AV\Lambda} \tag{A.2}$$

where $\mathbf{\Lambda}$ is a diagonal matrix of eigenvalues, and $\mathbf{V}$ is the matrix of eigenvectors.

Expanding $\tilde{u}$ into

$$\tilde{u} = \mathbf{V}y. \tag{A.3}$$

Substituting (A.3) into (A.1), then multiplying $\mathbf{V}^H$ on both sides, we obtain in a source-free problem

$$\mathbf{V}^H\mathbf{AV}\left(\frac{d}{dt}y - \mathbf{\Lambda}y\right) = 0. \tag{A.4}$$

Hence,

$$\frac{d}{dt}y - \mathbf{\Lambda}y = 0 \tag{A.5}$$

which is a fully decoupled system of equations. Consider an ith row of (A.5), which has $\lambda_i = e_i + jd_i$, it can be written as

$$\frac{d}{dt}y_i - (e_i + jd_i)y_i = 0. \tag{A.6}$$

After applying a forward-difference-based time discretization scheme to (A.6), we get

$$y_i^{n+1} - y_i^n - \Delta t\lambda_i y_i^n = 0. \tag{A.7}$$

Performing a z-transform of the above, we find

$$z = 1 + \Delta t\lambda_i. \tag{A.8}$$

To be stable, $|z| < 1$ should be satisfied, from which we obtain

$$(1 + \Delta te_i)^2 + (\Delta td_i)^2 < 1 \tag{A.9}$$

which yields

$$({e_i}^2 + {d_i}^2)\Delta t^2 + 2e_i\Delta t < 0. \tag{A.10}$$

Since $\Delta t > 0$, and the real part of the eigenvalue e_i is negative

$$\Delta t \le \frac{2|e_i|}{{e_i}^2 + {d_i}^2} = \frac{2\,|\mathrm{Re}[\lambda_i]|}{|\lambda_i|^2}. \tag{A.11}$$

REFERENCES

[1] D. Jiao and J. M. Jin, "A general approach for the stability analysis of time-domain finite element method," *IEEE Trans. Antennas Propag.*, vol. 50, no. 11, pp. 1624–1632, Nov. 2002.

[2] S. D. Gedney and U. Navsariwala, "An unconditionally stable finite-element time-domain solution of the vector wave equation," *IEEE Microw. Guided Wave Lett.*, vol. 5, pp. 332–334, May 1995.

[3] T. Namiki, "A new FDTD algorithm based on alternating-direction implicit method," *IEEE Trans. Microw. Theory Techn.*, vol. 47, no. 10, pp. 2003–2007, Oct. 1999.

[4] F. Zheng, Z. Chen, and J. Zhang, "A finite-difference time-domain method without the Courant stability conditions," *IEEE Microw. Guided Wave Lett.*, vol. 9, no. 11, pp. 441–443, Nov. 1999.

[5] C. Sun and C. W. Trueman, "Unconditionally stable Crank-Nicolson scheme for solving two-dimensional Maxwell's equations," *Electron. Lett.*, vol. 39, no. 7, pp. 595–597, Apr. 2003.

[6] Y. Chung, T. K. Sarkar, B. H. Jung, and M. Salazar-Palma, "An unconditionally stable scheme for the finite-difference time-domain method," *IEEE Trans. Microw. Theory Techn.*, vol. 51, no. 3, pp. 697–704, Mar. 2003.

[7] E. L. Tan, "Fundamental schemes for efficient unconditionally stable implicit finite-difference time-domain methods," *IEEE Trans. Antennas Propag.*, vol. 56, no. 1, pp. 170–177, Jan. 2008.

[8] M. Movahhedi and A. Abdipour, "Alternation-direction implicit formulation of the finite-element time-domain method," *IEEE Trans. Microw. Theory Techn.*, vol. 55, no. 6, pp. 1322–1331, Jun. 2007.

[9] C. D. Sarris, "Extending the stability limit of the FDTD method with spatial filtering," *IEEE Microw. Wireless Comp. Lett.*, vol. 21, no. 4, pp. 176–178, Apr. 2011.

[10] C. Chang and D. S. Costas, "A spatially filtered finite-difference time-domain scheme with controllable stability beyond the CFL limit," *IEEE Trans. Microw. Theory Techn.*, vol. 61, no. 1, pp. 351–359, Mar. 2013.

[11] Q. He, H. Gan, and D. Jiao, "Explicit time-domain finite-element method stabilized for an arbitrarily large time step," *IEEE Trans. Antennas Propag.*, vol. 60, no. 11, pp. 5240–5250, Nov. 2012.

[12] M. Gaffar and D. Jiao, "An explicit and unconditionally stable FDTD method for the analysis of general 3-D lossy problems," *IEEE Trans. Antennas Propag.*, vol. 63, no. 9, pp. 4003–4015, Sep. 2015.

[13] M. Gaffar and D. Jiao, "An explicit and unconditionally stable FDTD method for electromagnetic analysis," *IEEE Trans. Microw. Theory Techn.*, vol. 62, no. 11, pp. 2538–2550, Nov. 2014.

[14] F. Tisseur and K. Meerbergen, "The quadratic eigenvalue problem," *SIAM Rev.*, vol. 43, no. 2, pp. 235–286, 2001.

[15] D. C. Sorensen, "Implicit application of polynomial filters in a k-step arnoldi method," *SIAM J. Matrix Anal. Appl.*, vol. 13, pp. 357–385, 1992.

[16] Y. Saad, *Numerical Methods for Large Eigenvalue Problems.* Manchester, U.K.: Manchester Univ. Press, 1992.

[17] J. Lee, D. Chen, V. Balakrishnan, C.-K. Koh, and D. Jiao, "A quadratic eigenvalue solver of linear complexity for 3-D electromagnetics-based analysis of large-scale integrated circuits," *IEEE Trans. Comput.-Aided Design Integr. Circuits Sys.*, vol. 31, no. 3, pp. 380–390, Mar. 2012.

[18] W. Lee and D. Jiao, "An alternative explicit and unconditionally stable time-domain finite-element method for analyzing general lossy electromagnetic problems," in *Proc. IEEE Int. Conf. Comput. Electromagn.*, Guangzhou, China, 2016.

Woochan Lee (GS'14–M'15) received the B.S. and M.S. degrees in electrical engineering from Seoul National University, Seoul, Korea, in 2002 and 2005, respectively, and the Ph.D. degree in electrical and computer engineering from Purdue University, West Lafayette, IN, USA, in 2016.

He was commissioned as a Full-Time Lecturer and a First Lieutenant with the Korea Military Academy, Seoul, Korea, from 2005 to 2008. He was a Deputy Director and a Patent Examiner with the Korean Intellectual Property Office, Daejeon, South Korea, from 2004 to 2017. In 2017, he joined the Department of Electrical Engineering, Incheon National University, Incheon, South Korea, where he is currently an Assistant Professor. His current research interests include computational electromagnetics and machine learning applications for very large-scale electromagnetic analysis.

Dan Jiao (M'02–SM'06–F'16) received the Ph.D. degree in electrical engineering from the University of Illinois, Urbana–Champaign, IL, USA, in 2001.

She was then with the Technology Computer-Aided Design (CAD) Division, Intel Corporation, until September 2005, as a Senior CAD Engineer, Staff Engineer, and Senior Staff Engineer. In September 2005, she joined Purdue University, West Lafayette, IN, USA, as an Assistant Professor with the School of Electrical and Computer Engineering, where she is now a Professor. She has authored 3 book chapters and over 260 papers in refereed journals and international conferences. Her current research interests include computational electromagnetics, high-frequency digital, analog, mixed-signal, and RF integrated circuit (IC) design and analysis, high-performance VLSI CAD, modeling of microscale and nanoscale circuits, applied electromagnetics, fast and high-capacity numerical methods, fast time-domain analysis, scattering and antenna analysis, RF, microwave, and millimeter-wave circuits, wireless communication, and bioelectromagnetics.

Dr. Jiao has served as the Reviewer for many IEEE journals and conferences. She was the recipient of the 2013 S. A. Schelkunoff Prize Paper Award of the IEEE Antennas and Propagation Society, which recognizes the Best Paper published in the IEEE TRANSACTIONS ON ANTENNAS AND PROPAGATION during the previous year. She has been named a University Faculty Scholar by Purdue University since 2013. She was among the 85 engineers selected throughout the nation for the National Academy of Engineering's 2011 U.S. Frontiers of Engineering Symposium. She was the recipient of the 2010 Ruth and Joel Spira Outstanding Teaching Award, the 2008 National Science Foundation (NSF) CAREER Award, the 2006 Jack and Cathie Kozik Faculty Start Up Award (which recognizes an outstanding new faculty member of the School of Electrical and Computer Engineering, Purdue University), a 2006 Office of Naval Research (ONR) Award under the Young Investigator Program, the 2004 Best Paper Award presented at the Intel Corporation's annual corporate-wide technology conference (Design and Test Technology Conference) for her work on generic broadband model of high-speed circuits, the 2003 Intel Corporation's Logic Technology Development (LTD) Divisional Achievement Award, the Intel Corporation's Technology CAD Divisional Achievement Award, the 2002 Intel Corporation's Components Research the Intel Hero Award (Intel-wide she was the tenth recipient), the Intel Corporation's LTD Team Quality Award, and the 2000 Raj Mittra Outstanding Research Award presented by the University of Illinois at Urbana–Champaign.